

## Defect structures in the silver halides

D. J. Wilson,<sup>1,2,\*</sup> A. A. Sokol,<sup>1,2</sup> S. A. French,<sup>1,†</sup> and C. R. A. Catlow<sup>1,2,‡</sup>

<sup>1</sup>*Davy Faraday Research Laboratory, The Royal Institution of Great Britain, London, W1S 4BS*

<sup>2</sup>*Department of Chemistry, University College London, London, WC1H 0AJ*

(Received 2 July 2007; published 28 February 2008)

We report a state of the art density functional theory study of the intrinsic defects within the rocksalt-structured silver halides. These materials are well known to favor Frenkel defect pairs over Schottky pairs—a key factor in their use as photographic materials. We report the defect structures and formation energies of the elementary point defects obtained using the supercell approximation. In agreement with recent experimental results, we find that the interstitial cation adopts a split-interstitial configuration, centered on a lattice site. The effects of electron or hole trapping on the defect centers in AgCl and AgBr are reported, including the formation energetics, structures, and spin localizations. Although limitations in the supercell method are evident, we have nevertheless obtained valuable new insights into the properties of these fascinating materials.

DOI: [10.1103/PhysRevB.77.064115](https://doi.org/10.1103/PhysRevB.77.064115)

PACS number(s): 61.72.J–, 71.15.Mb, 71.23.An

### I. INTRODUCTION

The question of the structures of the intrinsic point defects in the silver halides is of both fundamental and industrial relevance. The silver halides are, of course, central to the photographic industry, largely due to their unique defect properties. While the majority of rocksalt-structured materials contain Schottky defect pairs, the dominant form in the silver halides are Frenkel defect pairs, consisting of interstitial cations and corresponding vacancies.<sup>1</sup>

The ease of formation of the interstitial cation, along with its subsequent high mobility within the crystalline lattice, are crucial to the efficiency of the photographic process. In a theory first proposed by Gurney and Mott in 1937,<sup>2</sup> and later refined by Berg,<sup>3</sup> Seitz,<sup>4</sup> and Hamilton<sup>5,6</sup> (amongst others), the process proceeds stepwise via electronic and ionic stages.

First, a conduction band electron, formed along with a hole upon excitation by incident light, becomes trapped at a positively charged ( $+\frac{1}{2}e$ ) surface kink site. The resultant negative static charge can then draw a bulk interstitial cation towards the surface. When they meet, recombination occurs, forming a neutral silver atom and regenerating the charged surface defect. Given a great enough photon flux, the process repeats until a stable silver cluster is formed. This cluster constitutes the photographic latent image, which can later be developed into a visible image.

The efficacy of this process relies, in part, upon the assumption that the electron-hole pair does not recombine. Experiments have shown that the positively charged hole becomes trapped very quickly.<sup>7</sup> At low temperatures the hole may become self-trapped; at elevated temperatures this species exists only if stabilized by a nearby negatively charged cation vacancy.<sup>8,9</sup> Recent low-temperature ENDOR studies on the isolated self-trapped hole (STH) in AgCl have suggested that it is localized over a central silver  $4d_{x^2-y^2}$  orbital and four surrounding chloride orbitals, forming a  $[\text{AgCl}_4]^{2-}$  unit.<sup>10</sup>

Within the bulk, it is thought that the electron can become trapped at an interstitial silver ion at low temperatures,<sup>11</sup> which has been verified by more recent experiments, with the trap having been found to be very shallow.<sup>12,13</sup> Conse-

quently, under normal operating conditions the mobility of the electrons will be unaffected by these centers, allowing them to reach surface traps rapidly. While most previous analyses have assumed the interstitial ion is located at a body-centered site, the ENDOR spectra have suggested that the neutral interstitial cation adopts a split-interstitial configuration with a neighboring cation, forming a  $\text{Ag}_2^+$  “molecule” within the lattice. This species was found to be centered upon a silver lattice site, orientated in a  $\langle 110 \rangle$  direction. It was suggested by the authors that the charged defect ( $\text{Ag}_2^{2+}$ ) would be of the same nature as the diffuse trapped electron and would not alter the structure significantly.

Despite interest in the silver halides, there have been relatively few theoretical studies of these materials, and even fewer which have dealt with defect properties. Classical atomistic techniques have provided key insights,<sup>14–18</sup> though they often relied upon unphysical parametrizations. The assumption in early calculations that the  $C_6$  term arose purely from van der Waals interactions relied heavily on a model of AgCl, in which ions were spherical and incompressible; this model was also extended further to include dipolar electronic polarization effects. However, the more complex nature of the physical interactions in these systems, such as those due to the hybridization of the silver  $4d$  orbitals with the  $p$  orbitals of neighboring halide anions,<sup>19</sup> often referred to as partial covalency, was neglected in this model. Further complex interactions arise from interionic penetration effects and changes of ion shape and size as a function of environment, which yield strong pure near-field electrostatic and polarization contributions to the interionic forces and the lattice energy, as in, for example, the successful modeling of quadrupole effects.<sup>20,21</sup>

Turning to electron structure techniques, the lack of electron correlation in Hartree-Fock methods has been shown to lead to a very poor representation of the pure silver halides.<sup>22</sup> Density functional theory (DFT) provides a much better description; however, previous studies have been limited to the examination of the unusual electronic structure of the material,<sup>23–27</sup> the elastic properties,<sup>27,28</sup> and the phonon properties.<sup>29</sup>

In this paper, we will expand our previous work<sup>30</sup> on intrinsic defects in silver chloride by studying the defect prop-

erties of all three rocksalt-structured silver halides (AgX), namely, silver fluoride (AgF), silver chloride (AgCl), and silver bromide (AgBr). We have used DFT to study the ground-state charged defect energetics and atomic structures, along with those of the corresponding neutral defects, in which an excess electron or hole is present. We have also calculated more accurate defect formation energies by employing a more sophisticated correction scheme, and by investigating the dependence of the properties on supercell size.

Our results, while illustrating some of the known limitations of periodic DFT calculations, provide valuable insight into the defect physics of these systems.

## II. METHOD

Our calculations used the CASTEP code,<sup>31</sup> which implements a combination of a plane wave basis set with pseudopotentials and periodic boundary conditions. The generalized gradient approximation (GGA) density functional of Perdew, Burke, and Ernzerhof<sup>32</sup> was chosen for its accuracy and numerical stability. The pseudopotentials, provided with the CASTEP code, were relativistically derived and consisted of core and valence regions of  $([\text{Kr}])4d^{10}5s^1$  for silver, and  $([\text{He}])2s^22p^5$ ,  $([\text{Ne}])3s^23p^5$ , and  $([\text{Ar}])3d^{10}4s^24p^5$  for fluorine, chlorine, and bromine, respectively.<sup>31,33</sup>

The convergence behavior of the defect formation energy as a function of both basis set size and  $k$ -point density has been examined in detail. All three materials showed the same trends, suggesting that the description of the cation was the limiting factor. As a consequence, the plane wave expansion was truncated at 350 eV for all three materials, which we have found to give convergence to within 0.01 eV. A Monkhorst-Pack grid of spacing  $0.03 \text{ \AA}^{-1}$  was used for the majority of the calculations, which corresponds to  $3 \times 3 \times 3$   $k$  points for a cubic 64 ion supercell and  $2 \times 2 \times 2$   $k$  points for a cubic 216 ion supercell. For most calculations, this number was drastically reduced by the application of symmetry. For our largest calculations, using 512 ion supercells, calculations were performed at the gamma point only.

The defect calculations were performed using the supercell approach, which has the advantage of simplicity, but has some well-known shortcomings.<sup>34–36</sup> Essentially this is a method for studying defects at high concentrations (i.e., at least one defect per supercell). However, it can be used to study isolated defects if the unwanted interactions between a defect and its periodic neighbors are in some way removed or corrected for. This approximation works well for defects with small multipole moments, but is less precise for cases such as charged defects in which there are significant long-range interactions. The monopole-monopole interactions can be removed *a posteriori* using the term of Leslie and Gillan,<sup>34</sup> while the dipole and quadrupole related terms have been derived by Makov and Payne.<sup>35</sup> When dealing with simple cubic supercells, the dominant correction terms are given by Eq. (1), where  $E_{corr}$  is the desired energy and  $E_0$  is the energy from the supercell calculation.

$$E_{corr}(L, q) = E_0 + \frac{\alpha q^2}{2L} + \frac{2\pi q Q}{3L^3} + O[L^{-5}]. \quad (1)$$

The second term on the right-hand side of Eq. (1) simply amounts to the energy of a system of periodic charges in a uniform background charge, where  $q$  is the defect charge and  $\alpha$  is the appropriate Madelung constant for this model system. The third term describes the interaction of the quadrupole ( $Q$ ) with the neutralizing background charge ( $q$ ). For the case of solid-state systems, where the defect-defect interactions are screened by polarization of the intervening ions, each term is reduced by the dielectric constant  $\epsilon$ . However, several recent studies have shown that while the monopole-monopole correction improves defect energetics, the accuracy of the monopole-quadrupole term depends strongly on the nature of the defect, and does not provide a consistent improvement.<sup>37,38</sup> Therefore, we have used this term only for the calculation of the energies of the isolated ions.

An alternative approach for solid-state systems was recently proposed by Castleton *et al.*,<sup>38</sup> in which Eq. (1) was simplified to

$$E_{corr}(L) = E_0 + \frac{a}{L} + \frac{b}{L^3} + O[L^{-5}], \quad (2)$$

on the basis that the defect-defect interactions must, to a first approximation, depend inversely upon their separation ( $L$ ), and the volume of the supercell ( $L^3$ ). Thus, with enough data, a value for  $E_0$  can be determined through a fitting procedure. However, bearing in mind that the dielectric constant will also vary with separation and volume,

$$\frac{1}{\epsilon} = \frac{1}{\epsilon_0} \left[ 1 + \frac{a'}{L} + \frac{b'}{V} + \dots \right], \quad (3)$$

we find that there should be an additional  $1/L^2$  term in the total energy,

$$E_{corr}(L) = E_0 + \frac{1}{\epsilon_0} \left[ \frac{a}{L} + \frac{aa'}{L^2} + \frac{b}{L^3} \right] + O[L^{-4}]. \quad (4)$$

In Sec. IV, values obtained using these extrapolation procedures are reported along with those corrected using the Leslie-Gillan term. As previously mentioned, these terms were applied *a posteriori*, and thus would not affect the calculation of forces, and thus the optimized geometry may therefore be inaccurate. In addition, these terms do not correct the electrostatic potential in the cell. As a consequence, electronic structure methods such as DFT will find the ground state of a perturbed system, and can thus report energies with large errors of the order of electron volts.<sup>39</sup> Schultz has proposed an alternative to the jellium compensating scheme, which correctly represents the electrostatic potential, and provides considerably more accurate defect energies.<sup>39,40</sup> However, his method requires a mixed boundary condition approach, and as such is incompatible with our plane wave basis set. In order to correct partially for this behavior, in our calculations of charged cells we adjusted the raw energies so that the semicore levels in the density of states lined up between pure and defective cells. The extent of this correction was of the order of 0.1 eV in all cases.

Additional correction terms are required when using arbitrary-shaped supercells due to noncancellation of certain multipole-multipole interactions.<sup>35,41</sup> Hence, for this work,

we have restricted our attention to the favorable case of the simple cubic supercells. For the majority of the calculations reported here, a cubic 64 ion supercell was used, of which only the inner 27 ions were allowed to relax, which is equivalent to relaxing up to and including the third-nearest neighbors, and involves fixing the positions of the ions on the cell boundary only. Individual defects were placed at the centre of the cell. For a limited subset of calculations, the next-largest cubic supercells of 216 and 512 ions were also employed. The increase in size was largely to combat the problems described above. However, we also relaxed one extra shell of ions in the 216 ion cell, taking the total number of active ions to 33. Symmetry was applied when appropriate to reduce the computational cost of these calculations. All calculations were performed at constant volume at the theoretically determined lattice parameters, which were all within 1% of their corresponding experimental values (see Sec. III A). Structures were considered relaxed when the residual force on each atom was less than  $0.05 \text{ eV}/\text{\AA}$ .

When calculating the full reaction cycle (i.e., the formation of a pair of charge-compensating defects) two-point defect formation energies are combined. Thus, for the cases of the cation Frenkel and Schottky defects, the resulting equations are, using Kröger-Vink notation,

$$\Delta E_F = E(\text{Ag}_i^\bullet) + E(V'_{\text{Ag}}) - 2E_{\text{pure}}, \quad (5)$$

$$\Delta E_S = E(V'_{\text{Ag}}) + E(V_X^\bullet) - \left(2 - \frac{1}{N}\right)E_{\text{pure}}, \quad (6)$$

where  $N$  is the number of  $\text{AgX}$  formula units in the pure cell.

For the Schottky pair, it is assumed the removed ions combine and add to the bulk material, and hence the sum of their chemical potentials can be replaced with the energy of a pair of ions in the bulk.

### III. PURE MATERIALS

#### A. Atomic structure

As an initial test of the reliability of these calculations, fundamental physical properties of the pure silver halides have been calculated. The cubic lattice parameters, the binding energies, the bulk moduli, and the three unique elastic constants  $C_{ij}$  are shown in Table I. All calculations employed a primitive unit cell with a converged  $k$ -point set. The elastic properties were obtained using the finite-strain technique.

As with other GGA-DFT calculations, the lattice parameters are systematically (slightly) overestimated, but are still within 1% of experimental values. Additionally, all three materials were found to be slightly overbound. The experimental values for the elastic properties of  $\text{AgCl}$  are extrapolated to absolute zero from data in the range 4.2–300 K (Ref. 44) and thus can be considered more accurate than the values quoted for  $\text{AgBr}$ , which are obtained from data in the range 273–673 K.<sup>45</sup> Given the nonlinearity at low temperatures found by the former authors, the quoted experimental values for  $\text{AgBr}$  can be considered only rough estimates, which may explain the apparent softness of  $\text{AgBr}$  in our calculations. To our knowledge, no experimental elastic data exist for  $\text{AgF}$ .

Given these results, we have confidence that our method more accurately represents the silver halides than the atomistic methods of previous defect studies.<sup>14,18</sup> These models, although fitted to structural and elastic data, failed to reproduce accurately the strong Cauchy violation ( $C_{12} \neq C_{44}$ ) shown in the data in the table, which is an indication that fundamental interactions were unaccounted for in the simple form of the interatomic potentials used in these studies. As we are interested in energy differences between cells of equal size, the effects of the observed overbinding will be significantly reduced. Furthermore, our results are in better agreement with experiment than earlier LDA calculations for  $\text{AgCl}$ ,<sup>43</sup> highlighting the need for gradient-corrected functionals.

#### B. Electronic structure

The calculated band structures of the three halides are shown in Fig. 1, while the key band parameters are tabulated and compared with experiment in Table I. While our results are in good agreement with previous DFT studies,<sup>43,46,47</sup> each having an indirect  $L \rightarrow \Gamma$  transition, as with all DFT calculations these band gaps are systematically underestimated.

For the case of the indirect band gap, improved results were obtained by performing two additional calculations per material: one with an additional electron and one where an electron has been removed. The band gap can then be calculated according to the equation  $\Delta E_{BG} = E[-] + E[+] - 2E[0]$ , where  $E[0]$  is the energy of the neutral system and  $E[-]/E[+]$  are the energies of the charged cells.

Silver fluoride has been found via the eigenvalue spectrum to be a negative indirect band gap material, where it should have a positive gap of 2.8 eV. It cannot, therefore, be considered a dielectric ionic material within DFT. Based on a positive direct band gap we nevertheless attempt calculation of the defect properties. In this approach we expect to reproduce, to a first approximation, the properties primarily controlled by the charge density distribution (i.e., formation energies and structure of charged defects). However, the properties of excited and localized electron and hole defect states would be unreliable.

### IV. CHARGED DEFECTS

Charged defects in the silver halides have been studied in the past using both experimental and theoretical methods. Ionic conductivity measurements have provided valuable information on defect migration,<sup>48,49</sup> while atomistic calculations have provided insights into defect formation<sup>14–16,18</sup> and have revealed the mechanisms of interstitial and vacancy migration.<sup>49,50</sup>

There have been relatively few *ab initio* studies of charged defects in ionic materials, which has been largely due to the problems associated with calculating the properties of charged defects in periodic boundary conditions (as discussed earlier). With advances in computing power, it is now possible to study these defects in large enough supercells that spurious contributions to the defect energy from the periodic images can be significantly reduced, especially

TABLE I. A comparison of calculated and experimental properties of the pure silver halides.

		AgF	AgCl	AgBr
Lattice parameter, $a/\text{\AA}$	Calculated	5.01	5.53	5.82
	Calculated (SIC-LDA) (Ref. 23)		5.53	5.71
	Experimental	(4.94) <sup>a</sup>	5.51	5.77
Binding energy/eV	Calculated	-9.85	-9.23	-9.08
	Experimental	-9.45	-8.93	-8.77
Bulk modulus/GPa	Calculated	58.8	50.4	40.2
	Experimental		51.3	49.6
$C_{11}$ /GPa	Calculated	75.7	67.3	55.6
	Calculated (LDA) (Ref. 43)		98	
	Experimental		75.9 <sup>b</sup>	75.5 <sup>c</sup>
$C_{12}$ /GPa	Calculated	50.3	41.9	32.5
	Calculated (LDA) (Ref. 43)		42	
	Experimental		39.1	36.7
$C_{44}$ /GPa	Calculated	-3.8	5.4	7.5
	Calculated (LDA) (Ref. 43)		1.3	
	Experimental		6.9	8.3
Direct band gap/eV	Calculated <sup>d</sup>	4.96	4.22	3.87
	Calculated (SIC-LDA) (Ref. 23)		4.5	3.1
	Calculated (LDA) (Ref. 46)		3.6	3.0
	Experimental (Ref. 24)	4.63	5.15	4.29
Indirect band gap ( $L \rightarrow \Gamma$ )/eV	Calculated <sup>d</sup>	-0.36	0.94	0.71
	Calculated <sup>e</sup>	0.52	1.73	1.84
	Calculated (SIC-LDA) (Ref. 23)		2.3	1.6
	Calculated (LDA) (Ref. 46)		1.3	1.3
	Experimental (Ref. 24)	2.8	3.245	2.684

<sup>a</sup>Room temperature value from Ott.<sup>42</sup>

<sup>b</sup>Elastic data for AgCl from the low-temperature data of Hidshaw *et al.*<sup>44</sup>

<sup>c</sup>Elastic data for AgBr extrapolated from the high-temperature data of Cain *et al.*<sup>45</sup>

<sup>d</sup>As determined from the eigenvalue spectrum.

<sup>e</sup>As determined from the equation  $\Delta E_{BG} = E[-] + E[+] - 2E[0]$ , as described in the text.

when used in conjunction with *a posteriori* correction schemes.

### A. Energy of formation

We have first considered three processes of defect formation, and their relative energetics:

(1) Addition of a silver ion to form an interstitial cation defect, again in Kröger-Vink notation as follows:



(2) Removal of a silver ion, leaving a cation vacancy as follows:

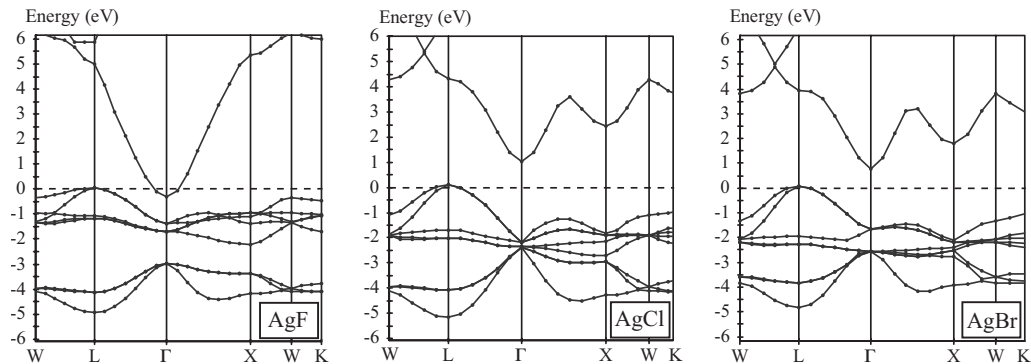
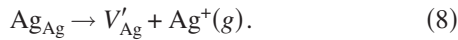


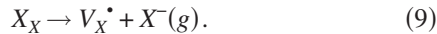
FIG. 1. Calculated band structures of the three rocksalt silver halides. Special points of the Brillouin zone:  $\Gamma = [0; 0; 0]$ ,  $X = [\frac{1}{2}; \frac{1}{2}; 0]$ ,  $K = [\frac{3}{8}; \frac{3}{8}; \frac{3}{4}]$ ,  $L = [\frac{1}{2}; \frac{1}{2}; \frac{1}{2}]$ ,  $W = [\frac{1}{2}; \frac{1}{4}; \frac{3}{4}]$ .

TABLE II. Defect formation energies for the silver halides (eV). The classic interatomic potential values are from Ref. 18. Absolute values of the defect energies for individual charged defects are given for completeness and should be combined to obtain physically meaningful properties.

		AgF	AgCl	AgBr
$\text{Ag}_I^\bullet$	DFT	-15.80	-16.49	-16.24
	Classical		-5.42	-5.88
$V'_{\text{Ag}}$	DFT	16.36	17.10	16.70
	Classical		6.88	6.92
$V_X^\bullet$	DFT	-6.37	-6.94	-6.59
	Classical		4.35	3.67
Frenkel	DFT	0.56	0.61	0.46
	Classical		1.46	1.05
	Experimental		1.45 (Ref. 51)	1.00–1.05
Schottky	DFT	0.16	0.94	1.02
	Classical		1.70	1.40
	Experimental		>1.5 (Ref. 1)	



(3) Removal of a halide ion, resulting in an anion vacancy as follows:



The halide interstitial was considered beyond the scope of this study, as it is by far the minority point defect species, and has not been experimentally observed.

The resulting defect energies, calculated using a 64 ion supercell, and corrected for monopole-monopole interactions, are reported in Table II. It should be noted that within approaches using periodic boundary conditions there is no unique way of defining such a quantity, as this process is one half of the full reaction, and it is in itself physically unreasonable. The values quoted here are simply the energies required to move the charged ion from the bulk to infinity. However, when these values are combined to form defect pairs, the results are well defined, experimentally verifiable quantities.

It can be seen from the tables that the dominance of the charged cation Frenkel pair for AgCl and AgBr is correctly predicted. Experimental data for the minority defect species are scarce due to the difficulty of the experiments involved, while data are not currently available for AgF as experiments are hindered by its tendency to absorb water. Our results for this material can therefore be considered as predictions.

All values are systematically lower in energy than would be expected, which is likely to be due to the inaccurate description of the electrostatic potential in the cell, as discussed in Sec. II. To our knowledge, the only available method for improving the quality of our results is to employ a larger supercell in which the periodic charged defects are further separated. In order to investigate this, we have performed key calculations using larger, and considerably more computationally expensive, 216 ion and 512 ion supercells. These

TABLE III. Defect formation energies for AgCl using 64 ion, 216 ion, and 512 ion supercells (eV).

		Raw	LG-Corrected
$\text{Ag}_I^\bullet$	64	-16.68	-16.49
	216	-16.44	-16.32
	512	-16.37	-16.28
	$1/L^2$	-16.3	
	$1/L^3$	-16.2	
	$V'_{\text{Ag}}$	64	16.90
216		17.15	17.28
512		17.17	17.26
$1/L^2$		17.2	
$1/L^3$		17.3	
$V_X^\bullet$		64	-7.13
	216	-7.29	-7.16
	512	-7.33	-7.24
	$1/L^2$	-7.3	
	$1/L^3$	-7.4	
	Frenkel	64	0.22
216		0.70	0.96
512		0.79	0.99
$1/L^2$		0.9	
$1/L^3$		1.1	
Schottky		64	0.55
	216	0.64	0.89
	512	0.61	0.80
	$1/L^2$	0.7	
	$1/L^3$	0.7	

calculations were only performed for silver chloride due to the large computational resources they require. The results are shown in Table III, along with the previously reported results for the smaller 64 ion cell. The values marked “ $1/L^3$ ” are estimates for infinite supercell size, based on Eq. (2), while those marked “ $1/L^2$ ” use the first two terms in Eq. (4) (the third was neglected due to lack of data in the fit).

From the extrapolation procedure, it is clear that terms of higher order than  $1/L$  are required. However, the choice between the  $1/L^2$  and  $1/L^3$  terms does not strongly affect the final defect energies (Table III). It would be very interesting to include both  $1/L^2$  and  $1/L^3$  terms in the fitting procedure, but we are limited by the small number of data points available from our calculations.

The results here suggest that the energetics derived from the 64 ion calculations are unreliable due to the large errors associated with the defect-defect interactions. Both the corrected and the extrapolated values for the Frenkel defect energy lie much closer to the experimental value (1.45 eV) than the results from the 64 ion cells. However, the energy of the Schottky pair is still much lower than experiment, where values >1.5 eV have been measured.<sup>1</sup>

While the calculation of the Frenkel defect energy simply involves summing the formation energies of the constituent point defects [Eq. (5)], the calculation of the Schottky defect

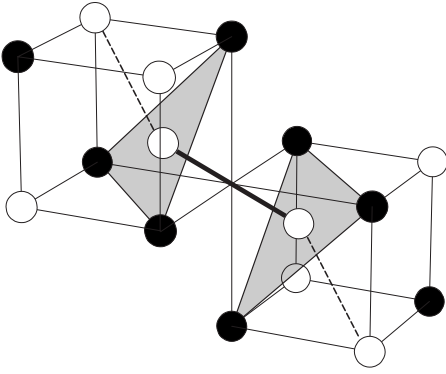


FIG. 2. Illustration of the charged  $\text{Ag}_2^{2+}$  split-interstitial species in the  $[111]$  orientation, with a typical cation chain highlighted. White circles represent silver ions. Black circles represent halide ions.

energy involves the crystal binding energy [Eq. (6)]. From Sec. III, we know that our calculated binding energies are too high. Therefore, we would expect that the use of the PBE exchange-correlation functional would bias our results towards favoring Schottky pairs over Frenkel pairs.

### B. Structure of the interstitial cation: $\text{Ag}_I^+$

The interstitial cation defect is of considerable interest as it is unusually mobile within the crystal and plays a key role in the photographic process. So far, all experimental conductivity data have been analyzed using a conventional body-centered (BC) model of the interstitial ion.<sup>48,52</sup> Energetics from classical atomistic calculations on charged interstitials also supported this assumption.<sup>14,15,18</sup>

Our calculations on all three halides have shown the BC structure to be unstable. Instead, we have found the equilibrium configuration to involve a second cation, forming a dumbbell-shaped split-interstitial structure centered on a lattice site (see Fig. 2), in agreement with both the Hartree-Fock results of Baetzold and Eachus for AgCl (Ref. 53) and the ENDOR work of Bennebroek *et al.* on AgCl and AgBr.<sup>12,13</sup>

However, there is disagreement over the orientation of this  $\text{Ag}_2$  species. Based on symmetry arguments, Bennebroek predicted a  $[110]$  orientation for the *neutral* defect in AgCl, and suggested that the charged defect should be qualitatively similar due to the diffuse nature of the trapped electron (with an effective radius estimated at  $16.6 \text{ \AA}$ ).<sup>13</sup> The orientation of the  $\text{Ag}_2^+$  species in AgBr could not be determined by the authors due to low spectroscopic resolution. Our calculations, in contrast, show that a  $[111]$  orientation is more stable in all three halides. Moreover, we find that the  $[110]$  orientation is unstable, and will relax back to a  $[111]$  configuration. Simple steric arguments suggest that a  $[111]$  orientation would be expected to be more favorable, which determined the choice of model Baetzold used for his Hartree-Fock calculations on AgCl.<sup>53</sup>

In our calculations, the bond length of the charged  $\text{Ag}_2^{2+}$  dimer was found to be  $2.95 \text{ \AA}$  in AgCl, with the silver ions located close to the centers of two triangles of chloride ions,

TABLE IV. Bond lengths in and around the  $\text{Ag}_2^{2+}$  dimer. Subscript “I” relates to the interstitial pair, while “L” relates to lattice site ions. All lengths are in  $\text{Å}$ .

	$\text{Ag}_2^{2+}$	$\text{Ag}_I-\text{Ag}_L$	$\text{Ag}_I-X_L$	$\text{Ag}_L-X_L$
AgF	2.69	2.76	2.28	2.50
AgCl	2.95	2.94	2.49	2.77
AgBr	4.11	2.89	2.64	2.91

as shown in Fig. 2. The distance between each member of the dimer and its nearest cation neighbors was found to be  $2.94 \text{ \AA}$ . We therefore observed chains of cations with approximately equal separation (indicated in Fig. 2), suggesting the importance of electrostatic energies in determining the structure. The slight inequality in the bond lengths is likely to be due to electrostatic interactions with the surrounding chloride anions, which were situated at a distance of  $2.49 \text{ \AA}$  from each cation ( $0.28 \text{ \AA}$  shorter than normal separation in pure AgCl, but with silver in a trigonal, rather than octahedral, configuration), displaced only slightly from their lattice sites ( $0.02 \text{ \AA}$  outwards) due to the competition between Coulombic attraction and short-range repulsion. Silver fluoride showed very similar behavior to AgCl, while AgBr had a significantly longer dimer bond length. All data are summarized in Table IV.

To validate this analysis, we performed calculations purely of the electrostatic energies. Atomic coordinates from our DFT calculations on each material were imported into the GULP code,<sup>54</sup> and assigned formal ionic charges. Variation of the electrostatic energy was calculated as a function of the  $\text{Ag}_2^{2+}$  dimer bond length, while keeping the remainder of the crystal fixed. This procedure gave an equilibrium bond length of  $2.7 \text{ \AA}$  for AgF,  $2.9 \text{ \AA}$  for AgCl, and  $3.1 \text{ \AA}$  for AgBr. The values for AgF and AgCl are very close to the DFT data, confirming that electrostatic interactions control the structure of these systems. That the DFT bond length for AgBr deviates so strongly from that of the electrostatic model suggests that steric effects become important due to the large size of the anion.

As an approximate measure of the ease of migration of the interstitial cation, we have studied the differences in energy between the relaxed  $[111]$  geometry and the relaxed geometry where the interstitial ion is constrained to be in a body-centered (BC) site, which represents the most likely transition state. As would be expected, in line with conductivity measurements, the barrier to migration was found to be very small. The barriers obtained by our method are shown in Table V. A direct comparison with experiment is not possible as all “experimental” data have been derived from actual measurements using a body-centered model of the equilibrium structure.<sup>55–57</sup> However, our results compare very favorably with the averaged interstitial defect mobility values quoted by Weber and Friauf.<sup>56</sup> A reinterpretation based on the split-interstitial model would be very useful, although, the analysis would be far more complex as the migration path shows a greater degree of correlation.

Previous atomistic calculations<sup>50,58</sup> have been used to study the difference in energy between the body-centered

TABLE V. Barriers to migration/eV.

	Calculated	Experimental <sup>a</sup>
AgF	0.49	
AgCl	0.06	0.05
AgBr	0.13	0.17

<sup>a</sup>Averaged interstitial defect mobility (Ref. 56).

and split-interstitial species in AgCl. As mentioned above, these calculations find the BC geometry to be of lowest energy, with a [111]-orientated transition state 0.03 eV higher in energy.<sup>59</sup> However, as stated in Sec. III, we consider our method more accurately represents the silver halides, and thus can be considered more reliable.

### C. Structure of the cation vacancy: $V'_{\text{Ag}}$

For the corresponding charged cation vacancy, we observe small structural relaxations, as reported in Table VI. We find that the distance between the vacancy center and nearest-neighbor anions increases, while the nearest silver ions relax inwards, as would be expected on electrostatic grounds.

### D. Structure of the anion vacancy: $V^*_X$

Although anion vacancies are relatively rare in these materials, they are of inherent interest. Anion vacancies are well-studied defects in the rocksalt-structured alkali halides, in which related  $F$  centers form readily<sup>60</sup> and data from the silver halides therefore provide a useful comparison.

The calculated relaxations are reported in Table VII. We find that while AgBr shows the expected behavior based on electrostatics, in contrast the nearest-neighbor cations in AgF and AgCl relax towards the vacancy.

This behavior is a further indication of the breakdown of the rigid ion model for these materials. It is clear that the

TABLE VI. Inward displacement of shells of nearest-neighbor (NN) ions towards charged cation vacancies in the silver halides (Å).

	First NN	Second NN	Third NN
AgF	-0.11	+0.08	0.00
AgCl	-0.10	+0.06	-0.04
AgBr	-0.12	+0.05	-0.02

TABLE VII. Inward displacement of shells of nearest-neighbor (NN) ions towards charged anion vacancies in the silver halides (Å).

	First NN	Second NN	Third NN
AgF	+0.34	+0.12	-0.02
AgCl	+0.04	+0.11	-0.02
AgBr	-0.06	+0.10	-0.01

fundamental interactions within the silver halides differ from those of the alkali halides. The  $p$ - $d$  hybridization, often referred to as partial covalency, shortens the cation-anion distance. On removal of an ion to form a vacancy, the nature of the bonding around the defect necessarily changes. Around an anion vacancy, our results imply that the bond-shortening effect is reduced, and therefore the nearest-neighbor cations must lower their energy by relaxing into the vacant space. The extent of this relaxation will be limited by the resultant changes in the electrostatic and short-ranged interactions. From the data in Table VII we can see that this balance shifts smoothly from AgF to AgBr.

## V. NEUTRAL DEFECTS

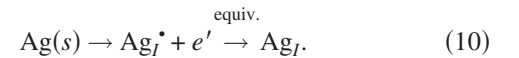
Neutral intrinsic defects in the silver halides consist of a hole or electron localized around a charged defect of opposite charge. These centers have direct relevance to the photographic process, as they determine the fate of the photoexcited electron-hole pair. For the photographic process to function efficiently, electrons must avoid traps in the bulk of the material before they reach their final surface trap. By contrast, holes must be trapped rapidly to avoid recombination.

As previously mentioned, due to the small concentrations of the other species, experimental studies have only been able to identify the individual defects associated with the Frenkel pair. Our calculations are not limited by these constraints, and therefore we can also study the formation of  $F$  centers ( $V_X^* + e^-$ ).

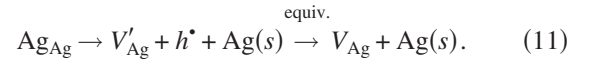
### A. Energy of formation

We now consider three new defect processes:

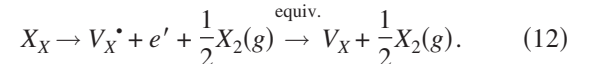
(1) Addition of a silver atom to form a neutral interstitial defect (which can be considered as an  $\text{Ag}^+$  cation and an excess electron) as follows:



(2) Removal of a silver atom leaving a vacancy and an excess hole as follows:



(3) Removal of a halogen atom resulting in an anion vacancy and an additional electron as follows:



The results of our calculations for AgCl and AgBr are reported in Table VIII. Calculations on the trapping properties of AgF were not carried out for the reasons stated in Sec. III.

Although the energies reported here can be considered to be more accurate than those of the charged defects, as all supercells were charge neutral, it is clear from the results for AgCl that we do not yet have convergence with supercell size. As will be described in the following section, this is due

TABLE VIII. Neutral defect formation energies for the silver halides (eV).

		AgCl	AgBr
$Ag_I$	64 ion	2.07	1.64
	216 ion	1.80	
$V_{Ag}$	64 ion	0.35	0.36
	216 ion	0.30	
$V_X$	64 ion	1.46	2.66
	216 ion	1.37	

to incorrect electron or hole localization due to finite-size effects.

It should be noted that these energies of formation are included for the sake of completeness. Concentrations of point defects in the bulk are determined by the formation energies of charged pairs. As has been previously discussed in the Introduction, there are no deep electron traps in the bulk, with trapping occurring predominantly at surface sites. Unfortunately, due to the aforementioned problems with modeling charged systems within a supercell, and the deficiencies of GGA functionals in reproducing the band gap, accurate trap depths could not be calculated using this technique. However, we have recently reinvestigated this problem using a sophisticated quantum mechanics/molecular mechanics (QM/MM) embedded cluster technique, the results of which will be reported in a subsequent publication.

### B. Structure of the interstitial cation: $Ag_I$

As described in the Introduction, ENDOR spectroscopy has identified a split-interstitial species in AgCl and AgBr, surrounded by a very diffuse trapped electron with Bohr radii of 16.6 and 24.8 Å, respectively.<sup>13</sup> The corresponding optimized structures and electron localizations found by us are displayed in Figs. 3 and 4. Our calculations predicted a small bond length increase of the  $Ag_2$  species to 3.00 Å for AgCl and 4.14 Å for AgBr, which was indicative of shallow trapping. While a full quantitative comparison with experiment

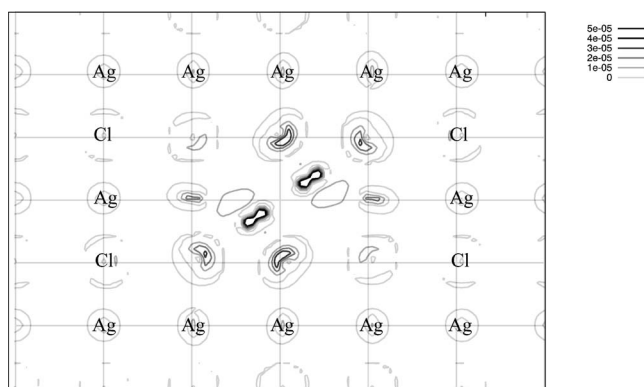


FIG. 3. Spin localization in defective AgCl: interstitial silver cation. Contour plot of the  $\langle 110 \rangle$  plane in the larger 217 ion supercell containing the  $Ag_2^+$  species (center). Vertices on the overlaid grid correspond to lattice sites.

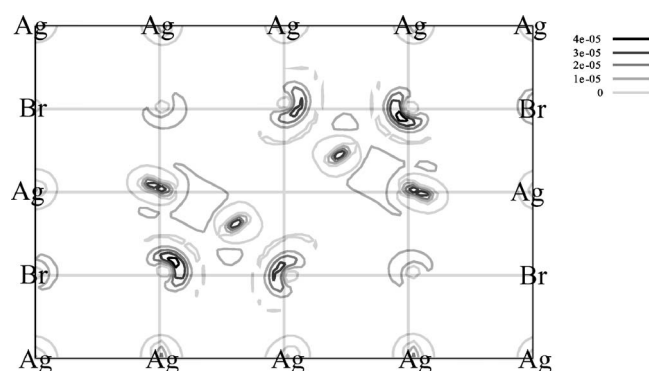


FIG. 4. Spin localization in defective AgBr: interstitial silver cation. Contour plot of the  $\langle 110 \rangle$  plane in the smaller 65 ion supercell containing the  $Ag_2^+$  species (center).

would require calculations on larger supercells capable of fully enclosing the electron density, we did observe diffuse localization in both cases.

In AgCl, it can be seen that the electron density, although diffuse, is somewhat concentrated upon  $p$ -like polarization functions of the two interstitial cations. In contrast, the increased dielectric constant of AgBr results in electron density that is spread across a larger  $Ag_2Br_8$  unit.

Some caution in the interpretation of our results is needed. GGA-DFT is well known to overdelocalize the electron distribution,<sup>61</sup> which may have the effect of increasing the bond lengths of the molecular ions in their neutral states, making the more constrained  $[110]$  geometries less favorable.

### C. Structure of the cation vacancy: $V_{Ag}$

The spin density for our 216 ion AgCl calculation is shown in Fig. 5, while the results for our 64 ion AgBr cal-

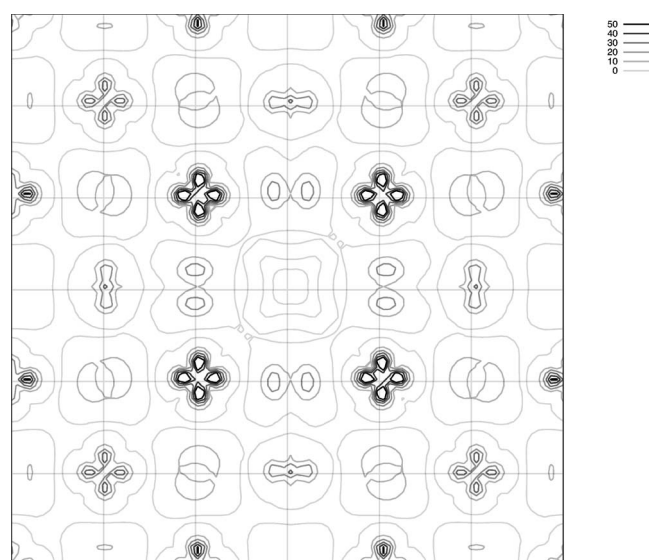


FIG. 5. Spin localization in defective AgCl: silver vacancy. Contour plot of a  $\langle 100 \rangle$  plane in the larger 215 ion supercell containing the vacancy (center).



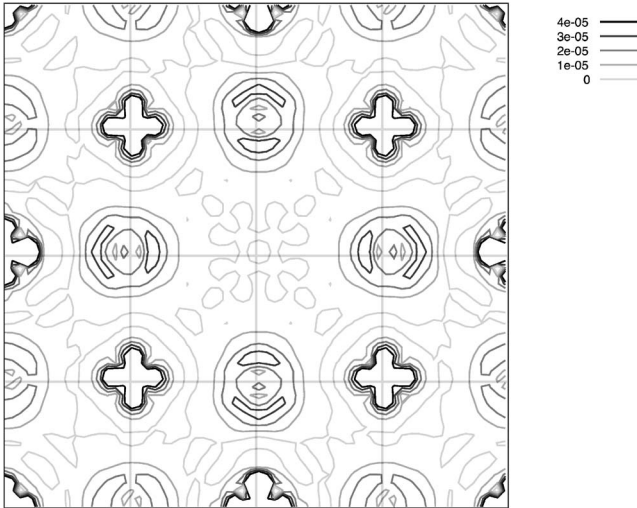


FIG. 6. Spin localization in defective AgBr: silver vacancy. Contour plot of a  $\langle 100 \rangle$  plane in the smaller 63 ion supercell containing the vacancy (center).

culations are displayed in Fig. 6. We see that the hole predominantly localizes on the silver cations, populating the  $d_{x^2-y^2}$  orbitals, and is found to be stable with respect to small symmetry-breaking perturbations of the nearest-neighbor ions. The magnitude of the relaxations are shown in Table IX which, as expected, are very similar to those for the charged cation vacancy (Table VI). Any differences are due to the slight change in fractional charge across the next-nearest-neighbor cations.

We note that both spin density patterns show appreciable density on cations around the cell boundary, which is due to the close proximity of the image defects, and would disappear in the limit of infinite dilution. Indeed, we observe this effect in moving from the 63 ion to the 215 ion AgCl supercells.

Previous experimental studies of the hole-vacancy complex in AgCl have suggested that the hole is centered on a *single* Jahn-Teller elongated lattice cation adjacent to the vacancy.<sup>9,62</sup> The difference in our distribution may be due to the localization problem in DFT. Pacchioni *et al.* have recently found that the hole in an  $\alpha$ -quartz Al center is incorrectly described by DFT.<sup>63</sup> Experiment and MP2 calculations showed localization on a single oxygen site, while hybrid and pure DFT methods showed the hole to be delocalized over a number of oxygen ions. More recent hybrid functionals<sup>64</sup> have, however, managed to reproduce experimental behavior.<sup>65</sup>

#### D. Structure of the anion vacancy: $V_X$

The electronic properties of vacancies at anion sites are of interest as they are deep electron traps. In the alkali halides,

TABLE IX. Inward displacement of shells of nearest-neighbor (NN) ions towards neutral silver vacancies in the silver halides ( $\text{\AA}$ ).

	First NN	Second NN	Third NN
AgCl	-0.09	+0.07	-0.04
AgBr	-0.14	+0.05	0.00

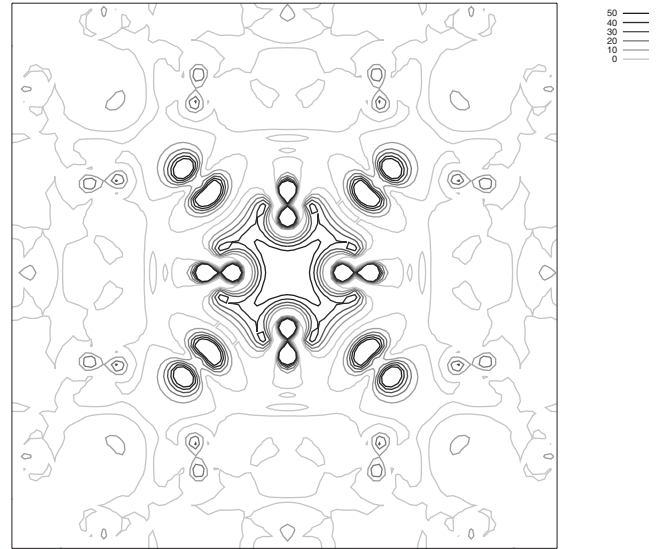


FIG. 7. Spin localization in defective AgCl: chlorine vacancy. Contour plot of a  $\langle 100 \rangle$  plane in the larger 215 ion supercell containing the vacancy (center).

an  $F$  center forms when an electron becomes trapped at an anion vacancy. It can be seen in Fig. 7 that a diffuse  $F$  center also forms in AgCl. However, the electron density is largely located upon the nearest-neighbor cations, rather than being concentrated within the vacancy itself as in a conventional  $F$  center. The situation was found to be very similar for AgBr; however, with its higher dielectric constant the electron density is more diffuse.

We see from Table X that trapping of an electron causes the neighbouring silver ions to contract symmetrically into the vacancy by  $0.70 \text{ \AA}$  for AgCl. Again, the radial displacement of the other ions is small. However, this could be due to the constraints imposed by the small size of the cell. When breaking the initial symmetry, the system relaxes back to the symmetrical geometry shown in the figure.

In the majority of systems studied previously,<sup>60,66</sup> the nearest-neighbor cations to the vacancy expand outwards. The unusual cation contraction observed in our calculations therefore warranted further examination.

To investigate, we used the methodology described here to study a well-known and extensively studied system. Sodium chloride (NaCl) was chosen owing to its apparent similarities to AgCl: being isostructural with a common anion, and lattice parameters that match to within  $0.1 \text{ \AA}$ . Using the same procedure as above, we studied the  $F$  center, and found a well-localized electron contained within the vacancy. We also observed small structural relaxations, with the nearest-neighbor cations moving outwards by  $0.025 \text{ \AA}$ . On removal

TABLE X. Inward displacement of shells of nearest-neighbor (NN) ions towards neutral anion vacancies in the silver halides ( $\text{\AA}$ ).

	First NN	Second NN	Third NN
AgCl	+0.70	+0.08	0.01
AgBr	-0.02	+0.09	0.00

of this trapped electron to form a charged defect, we find outward relaxation of the cations and inward relaxation of the nearest anions, consistent with the electrostatics and with magnitudes comparable with previous embedded-cluster calculations.<sup>67</sup>

Thus, we consider that our results for the silver halides are valid, and that the unusual inward relaxation around the anion vacancy in AgCl can again be attributable to the complex nature of the bonding in this material.

## VI. CONCLUSIONS

This paper has illustrated some difficulties with current DFT methodologies when applied to modeling defects in insulators. Nevertheless, we have gained interesting structural information on the point defects, including the prediction of a [111]-orientated split interstitial structure for the charged silver interstitial species. In addition, we have confirmed the presence of the neutral split-interstitial defect as predicted by Bennebroek *et al.* on the basis of their ENDOR spectra.<sup>13</sup> We have also observed unusual relaxations around the vacancies, which we consider reflect the complex nature of the bonding in these materials.

Our calculations have given interesting insights into the localization of electrons and holes around these point defects. Although no quantitative comparisons could be made with experiment due to the small size of our models, we found good qualitative agreement between our calculations and Bennebroek's ENDOR work. In contrast, we find that

our calculations incorrectly predict the localization of the hole around the cation vacancy. However, the observed behavior is consistent with other similar studies which have found that GGA-DFT tends to overdelocalize the trapped-hole state.

Within the supercell approximation, the only way to achieve a consistent improvement in the energetics would be to move to larger system sizes, which would both reduce the error arising from the defect-defect interactions, and would also provide more data for the *a posteriori* correction schemes. However, such calculations are currently prohibitively expensive.

An alternative to the supercell approximation is the use of a QM/MM embedded cluster approach, which would alleviate many of the problems described here, at the cost of additional complexity. Such calculations will be reported in a future publication.

## ACKNOWLEDGMENTS

D.J.W. would like to thank Eastman Kodak for funding, and Thomas Pawlik and Roger Baetzold for discussions related to this work. The authors would also like to acknowledge the UKCP consortium for access to the academic version of the CASTEP code. Computer resources on the HPCx and CSAR services were provided via our membership of the UK HPC Materials Chemistry Consortium and funded by EPSRC (portfolio Grant No. EP/D504872). Thanks also to Accelrys Inc., for the use of their Materials Studio visualization software.

\*Present address: Department of Geosciences, J. W. Goethe University, Frankfurt am Main, 60438 Germany.

†Present address: Johnson Matthey Technology Centre, Sonning Common, RG4 9NH, U.K.

‡c.r.a.catlow@ucl.ac.uk

<sup>1</sup>R. D. Fouchaux and R. O. Simmons, *Phys. Rev.* **136**, A1664 (1964).

<sup>2</sup>R. W. Gurney and N. F. Mott, *Proc. R. Soc. London, Ser. A* **164**, 151 (1938).

<sup>3</sup>W. F. Berg, *Trans. Faraday Soc.* **39**, 115 (1943).

<sup>4</sup>F. Seitz, *Rev. Mod. Phys.* **23**, 328 (1951).

<sup>5</sup>J. F. Hamilton, *Photograph. Sci. Eng.* **26**, 263 (1982).

<sup>6</sup>J. F. Hamilton, *Adv. Phys.* **37**, 359 (1988).

<sup>7</sup>J. Malinowski, *Photograph. Sci. Eng.* **14**, 112 (1970).

<sup>8</sup>H. Kanzaki and S. Sakuragi, *Solid State Commun.* **9**, 1667 (1971).

<sup>9</sup>C. T. Kao, L. G. Rowan, and L. M. Slifkin, *Phys. Rev. B* **42**, 3142 (1990).

<sup>10</sup>M. T. Bennebroek, A. v. Duijn-Arnold, J. Schmidt, O. G. Poluektov, and P. G. Baranov, *Phys. Rev. B* **66**, 054305 (2002).

<sup>11</sup>S. Sakuragi and H. Kanzaki, *Phys. Rev. Lett.* **38**, 1302 (1977).

<sup>12</sup>M. T. Bennebroek, O. G. Poluektov, A. J. Zakrzewski, P. G. Baranov, and J. Schmidt, *Phys. Rev. Lett.* **74**, 442 (1995).

<sup>13</sup>M. T. Bennebroek, A. Arnold, O. G. Poluektov, P. G. Baranov, and J. Schmidt, *Phys. Rev. B* **54**, 11276 (1996).

<sup>14</sup>C. R. A. Catlow, J. Corish, and P. W. M. Jacobs, *J. Phys. C* **12**, 3433 (1979).

<sup>15</sup>P. W. M. Jacobs, J. Corish, and B. A. Devlin, *Photograph. Sci. Eng.* **26**, 50 (1982).

<sup>16</sup>C. R. A. Catlow, J. Corish, J. H. Harding, and P. W. M. Jacobs, *Philos. Mag. A* **55**, 481 (1987).

<sup>17</sup>M. Bucher, *Phys. Rev. B* **30**, 947 (1984).

<sup>18</sup>R. C. Baetzold, C. R. A. Catlow, J. Corish, F. M. Healy, P. W. M. Jacobs, M. Leslie, and Y. T. Tan, *J. Phys. Chem. Solids* **50**, 791 (1989).

<sup>19</sup>J. A. Krumhansl, in *Photoconductivity Conference*, edited by R. G. Breckenridge, B. R. Russell, and E. E. Hahn (John Wiley & Sons, Inc., New York, 1956), p. 450.

<sup>20</sup>R. D. Banhatti and Y. V. G. S. Murti, *Phys. Rev. B* **48**, 6839 (1993).

<sup>21</sup>T. Tomoyose, A. Fukuchi, and M. Kobayashi, *Solid State Ionics* **167**, 83 (2004).

<sup>22</sup>E. Aprà, E. Stefanovich, R. Dovesi, and C. Roetti, *Chem. Phys. Lett.* **186**, 329 (1991).

<sup>23</sup>D. Vogel, P. Krüger, and J. Pollmann, *Phys. Rev. B* **58**, 3865 (1998).

<sup>24</sup>S. Glaus and G. Calzaferri, *Photochem. Photobiol. Sci.* **2**, 398 (2003).

<sup>25</sup>H. Overhof and U. Gerstmann, *Phys. Rev. B* **62**, 12585 (2000).

<sup>26</sup>G. S. Nunes, P. B. Allen, and J. L. Martins, *Solid State Commun.*

- 105**, 377 (1998).
- <sup>27</sup>T. Benmessabih, B. Amrani, F. El Haj Hassan, F. Hamdache, and M. Zoaeter, *Physica B* **392**, 309 (2007).
- <sup>28</sup>P. T. Jochym and K. Parlinski, *Phys. Rev. B* **65**, 024106 (2001).
- <sup>29</sup>Y. Li, L. Zhang, T. Cui, Y. Ma, G. Zou, and D. D. Klug, *Phys. Rev. B* **74**, 054102 (2006).
- <sup>30</sup>D. J. Wilson, A. A. Sokol, S. A. French, and C. R. A. Catlow, *J. Phys.: Condens. Matter* **16**, S2827 (2004).
- <sup>31</sup>S. J. Clark, M. D. Segall, C. J. Pickard, P. J. Hasnip, M. J. Probert, K. Refson, and M. C. Payne, *Z. Kristallogr.* **220**, 567 (2005).
- <sup>32</sup>J. P. Perdew, K. Burke, and M. Ernzerhof, *Phys. Rev. Lett.* **77**, 3865 (1996).
- <sup>33</sup>D. Vanderbilt, *Phys. Rev. B* **41**, 7892 (1990).
- <sup>34</sup>M. Leslie and M. J. Gillan, *J. Phys. C* **18**, 973 (1985).
- <sup>35</sup>G. Makov and M. C. Payne, *Phys. Rev. B* **51**, 4014 (1995).
- <sup>36</sup>G. Makov, R. Shah, and M. C. Payne, *Phys. Rev. B* **53**, 15513 (1996).
- <sup>37</sup>U. Gerstmann, P. Deák, R. Rurali, B. Aradi, T. Frauenheim, and H. Overhof, *Physica B* **340-342**, 190 (2003).
- <sup>38</sup>C. W. M. Castleton, A. Höglund, and S. Mirbt, *Phys. Rev. B* **73**, 035215 (2006).
- <sup>39</sup>P. A. Schultz, *Phys. Rev. Lett.* **84**, 1942 (2000).
- <sup>40</sup>J. Lento, J.-L. Mozos, and R. M. Nieminen, *J. Phys.: Condens. Matter* **14**, 2637 (2002).
- <sup>41</sup>L. N. Kantorovich, *Phys. Rev. B* **60**, 15476 (1999).
- <sup>42</sup>H. Ott, *Z. Kristallogr.* **63**, 222 (1926).
- <sup>43</sup>F. Kirchhoff, J. M. Holender, and M. J. Gillan, *Phys. Rev. B* **49**, 17420 (1994).
- <sup>44</sup>W. Hidshaw, J. T. Lewis, and C. V. Briscoe, *Phys. Rev.* **163**, 876 (1967).
- <sup>45</sup>L. S. Cain and G. Hu, *Phys. Rev. B* **64**, 104104 (2001).
- <sup>46</sup>R. H. Victora, *Phys. Rev. B* **56**, 4417 (1997).
- <sup>47</sup>B. N. Onwuagba, *Solid State Commun.* **97**, 267 (1996).
- <sup>48</sup>J. Corish and D. C. A. Mulcahy, *J. Phys. C* **13**, 6459 (1980).
- <sup>49</sup>B. A. Devlin and J. Corish, *J. Phys. C* **20**, 705 (1987).
- <sup>50</sup>P. W. M. Jacobs, J. Corish, and C. R. A. Catlow, *J. Phys. C* **13**, 1977 (1980).
- <sup>51</sup>J. K. Aboagye and R. J. Friauf, *Phys. Rev. B* **11**, 1654 (1975).
- <sup>52</sup>D. A. Keen, W. Hayes, and R. L. McGreevy, *J. Phys.: Condens. Matter* **2**, 2773 (1990).
- <sup>53</sup>R. C. Baetzold and R. S. Eachus, *J. Phys.: Condens. Matter* **7**, 3991 (1995).
- <sup>54</sup>J. D. Gale, *J. Chem. Soc., Faraday Trans.* **93**, 629 (1997).
- <sup>55</sup>J. Corish and P. W. M. Jacobs, *J. Phys. Chem. Solids* **33**, 1799 (1972).
- <sup>56</sup>M. D. Weber and R. J. Friauf, *J. Phys. Chem. Solids* **30**, 407 (1969).
- <sup>57</sup>J. E. Hove, *Phys. Rev.* **102**, 915 (1956).
- <sup>58</sup>A. K. Shukla, S. Ramdas, and C. N. Rao, *J. Solid State Chem.* **8**, 120 (1973).
- <sup>59</sup>J. Corish, *J. Chem. Soc., Faraday Trans. 2* **85**, 437 (1989).
- <sup>60</sup>A. M. Stoneham, *Theory of Defects in Solids* (Oxford University Press, New York, 1975).
- <sup>61</sup>J. L. Gavartin, P. V. Sushko, and A. L. Shluger, *Phys. Rev. B* **67**, 035108 (2003).
- <sup>62</sup>R. S. Eachus, T. D. Pawlik, and R. C. Baetzold, *J. Phys.: Condens. Matter* **12**, 8893 (2000).
- <sup>63</sup>G. Pacchioni, F. Frigoli, D. Ricci, and J. A. Weil, *Phys. Rev. B* **63**, 054102 (2000).
- <sup>64</sup>Y. Zhao, B. J. Lynch, and D. G. Truhlar, *J. Phys. Chem. A* **108**, 2715 (2004).
- <sup>65</sup>J. To, A. A. Sokol, S. A. French, N. Kaltsoyannis, and C. R. A. Catlow, *J. Chem. Phys.* **122**, 144704 (2005).
- <sup>66</sup>A. L. Shluger, A. S. Foster, J. L. Gavartin, and P. V. Sushko, in *Nano and Giga Challenges in Microelectronics*, edited by J. Greer, A. Korkin, and J. Labanowski (Elsevier, New York, 2003), pp. 151–222.
- <sup>67</sup>P. V. Sushko, Ph.D. thesis, University of London, 2000.